

OPEN ACCESS

Electromagnetic Resonance in Biological Form: A Role for Fields in Morphogenesis

To cite this article: Alexis M Pietak 2011 *J. Phys.: Conf. Ser.* **329** 012012

View the [article online](#) for updates and enhancements.

You may also like

- [Rapid, high-resolution measurement of leaf area and leaf orientation using terrestrial LiDAR scanning data](#)
Brian N Bailey and Walter F Mahaffee
- [Modeling and experimental validation of buckling dielectric elastomer actuators](#)
Rocco Vertechy, Antonio Frisoli, Massimo Bergamasco et al.
- [Finite Element Analysis of Nanoindentation and Elastic Behavior of Bi₂Te₃ Two-Dimensional Nanosheets](#)
Melissa Mathews, Hung-Ta Wang and Lin Li



ECS
The
Electrochemical
Society
Advancing solid state &
electrochemical science & technology

DISCOVER
how sustainability
intersects with
electrochemistry & solid
state science research

Electromagnetic Resonance in Biological Form: A Role for Fields in Morphogenesis

Alexis M Pietak

Kingston, Ontario, Canada, K7L 4V3

alexis.pietak@gmail.com

Abstract. In morphogenesis, the mechanisms through which homogeneous, symmetric collectives of self-same cells are able to consistently and precisely establish long-range pattern remain an open question of scientific research. This work explores the hypothesis of developing biological structures as dielectric microwave resonators, using plant leaves as a working example. A finite element analysis (FEA) model was designed to determine if suitable resonant modes were physically possible for geometric and electrical parameters similar to those of developing leaf tissue. Using the FEA model, resonant EM modes with patterns of relevance to developing leaf vein modalities were detected. Here I show how the single physical mechanism of EM resonance can self-consistently account for different kinds of key symmetry-breaking operations characteristic of a variety of leaf vascular patterns. On account of the existence of shared geometric signatures in a leaf's vascular pattern and the electric field component of EM resonant modes supported by a leaf-like structure, further theoretical and experimental investigations are warranted. Significantly, this hypothesis is not limited to leaf vascular patterning, but may be applicable to a variety of morphogenetic phenomena in a number of living systems.

1. Introduction

The diverse, intricate, and even mathematically precise patterns of many life forms are fascinating. Plants, for instance, have been called “living crystals” on account of the systematic patterning inherent in the placement of seeds, leaves, and branches [2]. Plant leaves, ubiquitous features of our everyday lives, actually exhibit an incredible wealth of intricate and rather precise patterns in their macroscopic vascular tissue structure (Figure 1). Interestingly, the main features of many leaf vascular patterns show long-range global symmetries and periodicities that can be mapped in relation to sets of nested circles [1] (Figure 2). The features of leaf patterns are therefore consistent with a holistic description in terms of a wave pattern, where each circle (or quasi-circle) is a wave-front [1]. In addition, some plant leaves show strikingly precise angular symmetry in the development of main axes (Figure 1 G-I). On account of these observations involving global features interrelated in systematic ways, a leaf pattern can be understood in terms of a field [1].

What makes biological patterns, such as those found in leaf vasculature, particularly awe inspiring is that they self-assemble from a macroscopically homogeneous and typically quite symmetrical initial

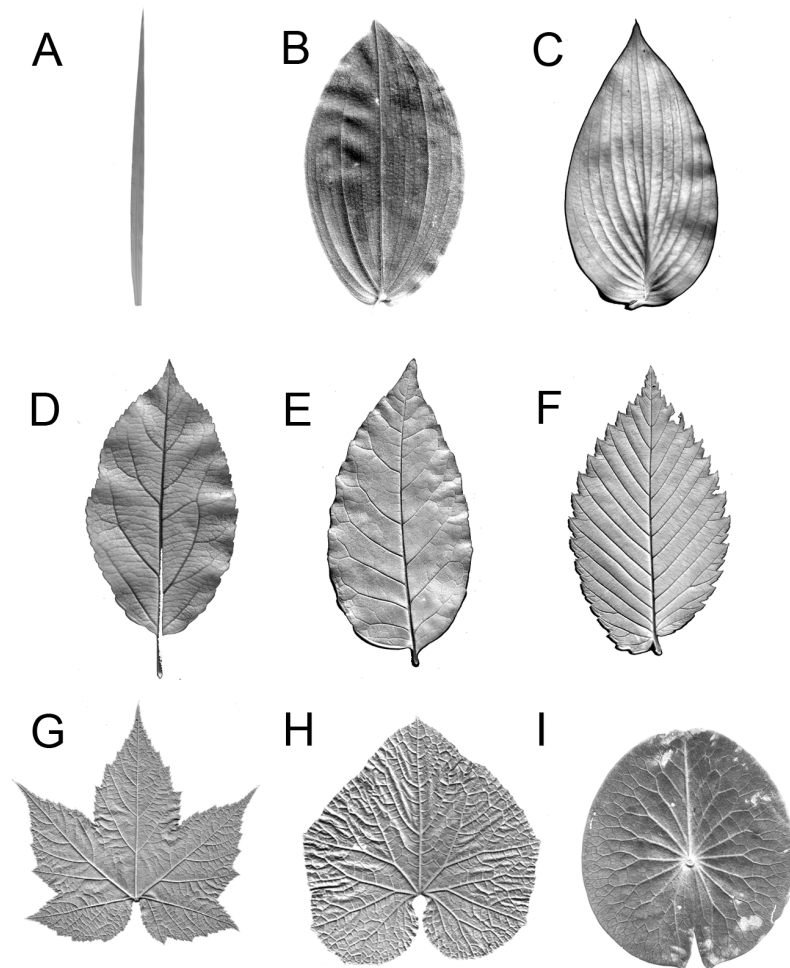


Figure 1: Plant leaves exhibit a wide variety of interesting vascular patterns. The top row shows leaves with a set of veins running roughly parallel to the central midvein, characteristic of pattern class 1 and monocots (panel A, crabgrass; panel B, twisted stalk; and panel C, hosta). The middle row shows leaves with secondary veins running at an angle to a central midvein, characteristic of pattern class 2 and dicots (panel D, apple; panel E, red ash; panel F, American beech). The bottom row shows pattern class 3 leaves with multiple major axes separated by a common angle (panel G, purple bush raspberry; panel H, zucchini; panel I, North American water lily).

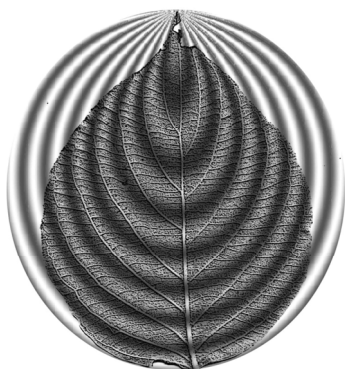


Figure 2: Many patterns in plant vasculature can be described in relation to a set of nested circular or quasi-circular forms with periodic or quasi-periodic spacing reminiscent of wave patterns. Shown here is the leaf of flowering dogwood with a wave pattern superimposed on top of the image [1]. Note how secondary vein spacing is specified by the wave's periodicity and how secondary veins tend to follow the trajectory of the wave fronts.

state where cells in the collective initially appear and behave in nearly identical ways. While today many of the self-assembly processes of morphogenesis can be handled using various complex systems models involving coupled reactions between cells, molecules, and genetic expression [3, 4], large gaps remain in our understanding of even basic morphogenetic phenomena.

The development of long-range patterns in leaf vasculature remains an example of such a gap in understanding. At a cellular level, it's been shown that flow of the plant hormone auxin through cells ultimately leads to their differentiation towards vascular tissue [5-7]. Essentially, while auxin can enter cells, it has trouble leaving without the help of a protein called PIN1 [5]. PIN1 is allocated to the boundary of cells and its positioning leads to the formation of auxin conduits [5]. This set-up is formally called the *auxin canalization mechanism* [6, 8]. PIN1 may be positioned in cells according to the flow of auxin through the cell [9]. This creates a positive feedback loop which results in the formation of dedicated auxin channels. These dedicated auxin channels in the meristematic tissue of the leaf primordium ultimately go on to differentiate into procambrial tissue, which ultimately becomes the vascular tissue system [5]. However, aspects of this hypothesis remain indeterminate because cellular auxin flux centers have still not been discovered, so it is unclear how cells can sense auxin flow to allocate PIN1 expression. Moreover, in almost thirty years of modeling, this interplay between auxin and PIN1 can generate little more than the primary midvein of a leaf and a scattered assembly of secondary veins [9], and certainly not the precise hierarchical organization of secondary and tertiary veins observed in a variety of real leaves [1]. Another mystery of leaf vascular development are experimental and theoretical indications that long-range vascular patterns grow from an array of high concentration auxin nodes forming in the leaf margin [10, 11]. Algorithms producing realistic depictions of leaf vascular patterns have utilized networks of nodes to account for complex vein configurations in leaves [12]. There remains, however, no indication of how auxin nodes form in the precise configurations in space and time that are required to account for leaf vascular patterns.

This present work explores an entirely new physical mechanism for morphogenesis in hypothesizing that fundamental symmetry-breaking operations occurring early in development, such as the appearance of high concentration auxin nodes at the margin of leaf primordia, could occur in response to spatially-patterned EM radiation forming within a developing organ structure. In fact, the field-like characteristics of a biological pattern, where global features show systematic interrelationships (Figure 1 and 2) can be explained if we understand the final pattern in relation to a resonant mode forming inside the developing organ structure. Resonant modes are standing wave patterns forming when a wave is confined within some kind of container and subjected to reflection from internal boundaries [13]. At internal boundaries, incident and reflected waves combine with one another to form a new pattern, the resonant mode, within the bulk material containing the waves. The resonant mode forms only at specific resonant frequencies, and is highly dependent on the geometry of the wave's container and the properties of waves travelling within the bulk material.

On account of their high water content and the polarity of other constituents like amino acids, many biological tissues have moderately high dielectric constants in the microwave regime [14-16]. For instance, human smooth muscle has a relative dielectric constant (ϵ_r) of 40 to 65 for frequencies of 1 to 10 GHz, decreasing to 7.5-9 at 100 GHz [16]. The ϵ_r of a 7% saline solution mimicking the ionic strength of plant juices, as well as juices extracted from corn stalks, were measured as 40 at 20 GHz [15]. And plant leaves (at 86 wt% water content) have ϵ_r of ~ 35 between 1 and 20 GHz [15]. As a developing plant is typically surrounded by weakly dielectric air ($\epsilon_r=1$), any radiation produced within the plant (and able to propagate within it) at frequencies high enough to generate wavelengths smaller than the plant organ should reflect from the internal air-plant interface, leading to the formation of an EM resonant mode within the plant. As these resonant modes are standing wave patterns with amplitudes and lines of force varying in space over a long-range, the EM mode could be a basic symmetry-breaking mechanism in the developing organ, defining the location of cellular differentiation, orientation, or expression of biomolecular substances such as auxin. Of course, a strong dielectric loss characteristic is also expected for microwave radiation in watery tissue, so from a classical perspective this hypothesis of biological forms as dielectric resonators should be impossible.

Thus, this model rests on the validity of biological coherence theories as described by Frohlich [17-19] and/or quantum field theorists [20-23].

The concept of coherence in biological systems makes the electromagnetic phenomena needed to create resonant modes within the container of a developing organ at least a theoretical possibility. In 1968, esteemed physicist Herbert Frohlich presented a theory implying the possibility of long-range coherence in thermodynamically open, far from equilibrium, and dissipative biological systems [17-19]. Coherence domains are a key concept that has developed from Frohlich's initial theory [21]. To use the simplest, crudest picture possible, coherence domains are regions of coherently (*i.e.* synchronized) oscillating charged biomolecules like water or cell structures such as cytoskeletal microfilaments. Because these oscillating structures are electrically charged, a coherent EM field is thought to be associated with their coherent vibration.

There are three key features proposed for coherence domains which enable the hypothesis of biological structures as dielectric resonators. First of all, coherence domains are proposed to form fields at frequencies in the microwave to sub-millimeter wave regions of the electromagnetic spectrum [24, 25]. This is important because radiation in this frequency range could form resonant mode patterns with spatial features relevant to those of developing biological features (in the range of 0.1 to 1 mm). Second of all, coherence domains have been hypothesized to be nearly lossless within the coherence domain [21, 26, 27] and mechanisms for EM signal propagation within a coherent biological system have been put forth [28]. This is important, as from a classical standpoint, the dielectric loss tangent and absorption characteristics of biological tissue are too high to sustain or propagate an EM resonant mode in the microwave-terahertz range [14, 15, 29]. Finally, very large coherent regions have been thought possible [30]. The hypothesis of biological structures as microwave resonators requires coherence domains spanning the range of the developing organ (~0.5-10 mm) as again, from a classical standpoint, microwave-terahertz radiation should not be able to travel any significant distances in a biological tissue due to its high loss and absorption characteristics, and would therefore probably not be able to reach boundaries, reflect, and interfere to form a resonant pattern unless the entire region exhibits coherence.

A previous report has examined the basic feasibility of plant leaves as dielectric microwave resonators [31]. This previous report used finite element analysis (FEA) to examine the form of resonant patterns forming on thin, pointed, elliptical disks with different width to length ratios [31]. The quality factors (Q-factors) of EM resonances on the different leaf-shaped models were measured while parameters such as the dielectric constant, conductivity, dielectric loss tangent, and thickness to length ratio of the models were varied. The results found that, with the exception of the dielectric loss tangent, the expected dielectric constants, conductivities, and thickness-to-length ratios of leaf tissue were in ranges capable of supporting EM resonant modes in the microwave frequency range [31]. In addition, as developing leaf primordia often form in a configuration where they are folded along the midvein, this previous report also explored the effect of folding on resonant pattern formation, which was determined to be minimal [31].

This present report builds on previous work as a more systematic assessment of EM resonant mode patterns forming on model geometries simulating possible developing leaf geometries. Here a more comprehensive comparison is made between EM resonant modes and actual leaf patterns. The single physical mechanism of EM resonance is shown capable of accounting for many different kinds of core symmetry-breaking operations observed in different kinds of leaf vascular pattern.

2. Methods

2.1. Finite Element Analysis Modelling

A finite element analysis (FEA) model based on the same reasoning outlined previously [31] was used to identify EM resonant modes on dielectric structures simulating developing leaves. The eigenmode solver of Ansoft HFSS 13.0 software (Ansys, USA) was utilized. The FEA model focused on four geometries: (i) model A, a pointed ellipse with a length three times its width; (ii) model B, a pointed ellipse with a length twice its width; (iii) model C, a pointed ellipse with a length nearly equal to its width; and (iv) a circle with equivalent length and width. Each model had a length of 8 mm (maximum dimension), a thickness of 200 μm , and a width prescribed by the model type. All models used a dielectric constant of 35, a dielectric loss tangent of zero, and bulk conductivity of zero. The model used resistive boundaries at 10 kOhm/mm. Note that finite dielectric loss tangents up to 0.05, bulk conductivities up to 5 S/m, and boundaries with a finite conductivity up to 5 S/m were also used in models and found to make no significant difference in the form of resulting EM modes, affecting only their Q-values. Finite element meshes were created using the automatic meshing routines of the HFSS software with mesh operations set to limit a maximum possible element length of 400 μm . The resulting FEA meshes depended on the model type and the frequency of excitation, with lower frequencies generating larger wavelengths and requiring fewer mesh elements for an accurate solution. Simulations at 20 GHz and above used meshes with more than 10,000 (and a maximum of 40,000) tetrahedral mesh elements. The simplest simulations utilized meshes with only 2232 tetrahedrons (model A), 2206 (model B), 5492 tetrahedrons (model C), and 4685 tetrahedrons (circle). These low order meshes were only used for the lowest frequencies (below 15 GHz). The three main models (model A, B, and C) and their lowest order meshes are shown in Figure 3.

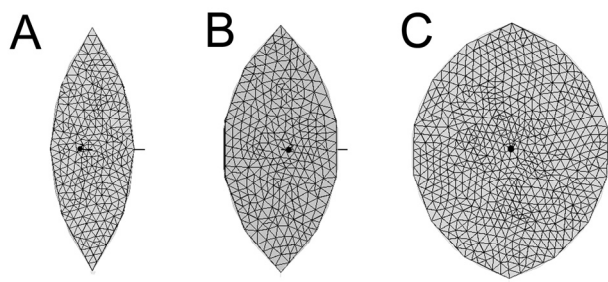


Figure 3: Three basic geometric models and the lowest quality meshes used in finite element analysis. Panel A shows model A, Panel B model B, and Panel C shows model C.

2.2. Leaf Vascular Pattern Analysis

Plant material was collected from 30 different randomly chosen species from the Great Lakes region of Canada (Kingston, Ontario, Canada) with common and Latin names listed in Table 1. Ten leaf samples from each species were digitally scanned (Canoscan Lide 20, Canoscan Inc, USA). Leaf images were measured using image-analysis software (ImageJ 1.37v). The 30 species listed in Table 2 represent a reference library of plant leaf patterns consulted in this work.

In this work, three basic pattern classes were defined for leaf vascular patterns. Pattern class 1 refers to the modality of parallel veins spanning from tip to petiole found in most monocot species, with examples shown in Figure 1 A-C. Pattern class 2 refers to a pattern commonly found in dicot plants characterized by a set of periodically (or quasi-periodically [1]) spaced secondary veins running at an angle off of a primary midvein, with examples shown in Figure 1 D-F. Pattern class 3 refers to a more complex modality characterized by the presence of 3 or more major axis (primary veins) separated by an even angular spacing, with a similar pattern repeated along each axis in the compound leaf (Figure 1 G-I).

Measurements of leaf margin, as defined by the first bifurcation point of secondary veins in pattern class 2 leaves, were made on five samples from each species at the point of maximum leaf width. Averages and standard error of the mean are reported.

Leaf pattern	Pattern Class
Crabgrass (<i>Digitaria sanguinalis</i>)	1
Hosta (<i>Hosta capitata</i>)	1
Twisted Stalk (<i>Streptopus amplexifolius</i>)	1
Apple tree (<i>Pyrus malus</i>)	2
American red raspberry (<i>Rubus idaeus</i>)	2
Common ragweed (<i>Ambrosia artemisiifolia</i>)	2
Northern Catalpa (<i>Catalpa speciosa</i>)	2
Poplar (<i>Populus fastigiata</i>)	2
American Beech (<i>Fagus grandifolia</i>)	2
Basswood (<i>Tilia Americana</i>)	2
Bitternut hickory (<i>Carya cordiformis</i>)	2
Common milkweed (<i>Asclepias syriaca</i>)	2
Flowering Dogwood (<i>Cornus canadensis</i>)	2
Horsechestnut (<i>Aesculus hippocastanum</i>)	2
Marsh milkweed (<i>Asclepias incarnata</i>)	2
Slippery elm (<i>Ulmus fulva</i>)	2
Staghorn sumac (<i>Rhus typhina</i>)	2
White Ash (<i>Fraxinus americana</i>)	2
Red Ash (<i>Fraxinus pensylvanica</i>)	2
White Elm (<i>Ulmus americana</i>)	2
White Birch (<i>Betula papyrifera</i>)	2
White Oak (<i>Quercus alba</i>)	2
Witch Hazel (<i>Hamamelis virginiana</i>)	2
Canada Moonseed (<i>Menispermum canadense</i>)	3
N. A. Water Lily (<i>Nymphaea odorata</i>)	3
Sugar maple (<i>Acer saccharum</i>)	3
Wild Grape (<i>Vitis riparia</i>)	3
Zucchini (<i>Cucurbita pepo</i>)	3
Common Geranium (<i>Pelargonium hortorum</i>)	3
Purple-flowering Raspberry (<i>Rubus odoratus</i>)	3

Table 1: List of plant species, Latin names, and pattern class designation for leaf vascular patterns considered in the present work.

3. Results

The electric field magnitudes of the first ten resonant modes forming in the four models are shown in Figure 4. In all EM modes, the electric field was parallel to the boundary of the flat disks, while the magnetic field assumed an angle out of the plane. Numerous EM mode patterns were seen in the four model geometries, all of them iterations upon common pattern modalities. Only the perfect circle

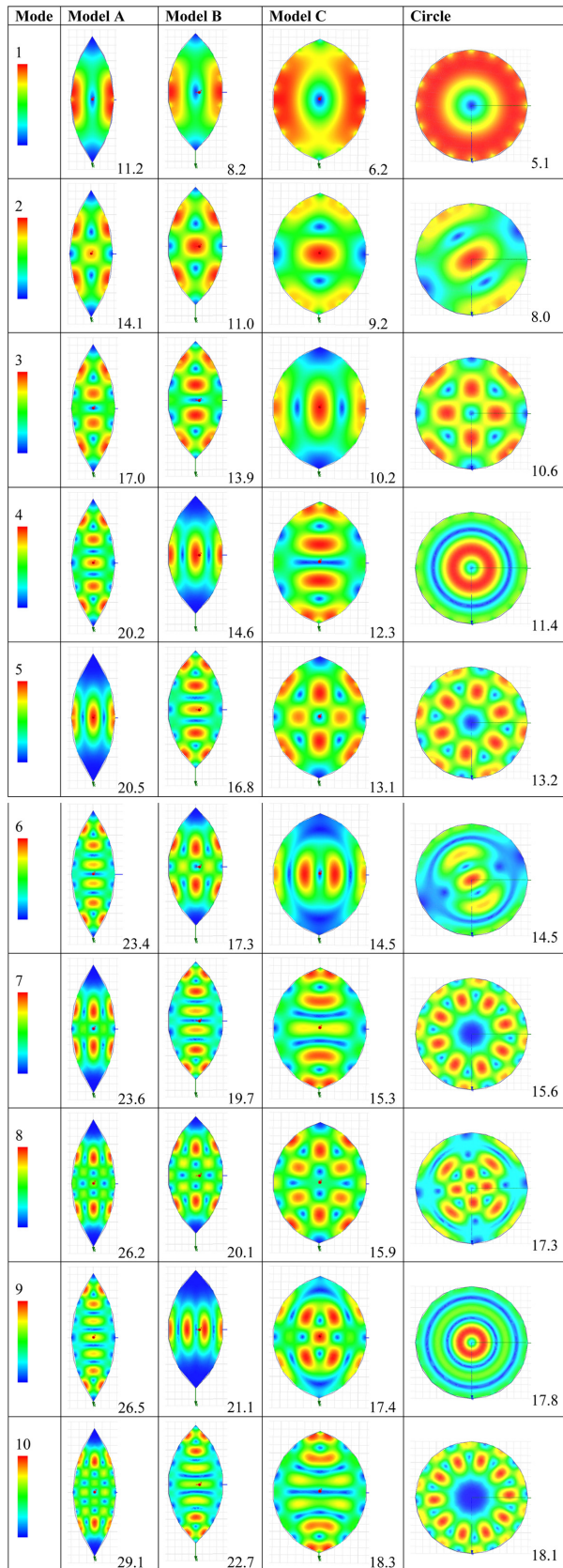


Figure 4: The electric field magnitude of the first ten resonant modes forming in the four geometric models. The bar to the left of each row shows the colour map, with red representing highest field strength and blue the lowest. All models have a length of 8 mm, thickness of 200 μm , and width prescribed by the model. All models used a dielectric constant of 35, conductivity and loss tangent set to zero, and resistive boundary conditions.

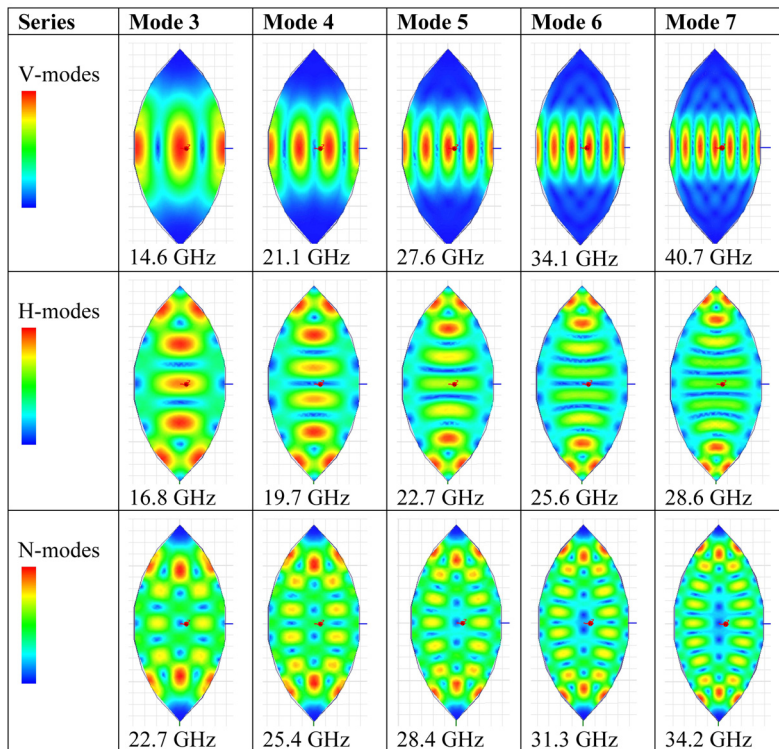


Figure 5: Resonant mode pattern series on model B. Top row shows the electric field strength of the V-mode series. Middle row shows the electric field strength of the H-mode series. Bottom row shows the electric field strength of the N-mode series. Beneath each image the resonant frequency is shown. The bar to the left of each row shows the colour map with red representing highest field strength and blue the lowest.

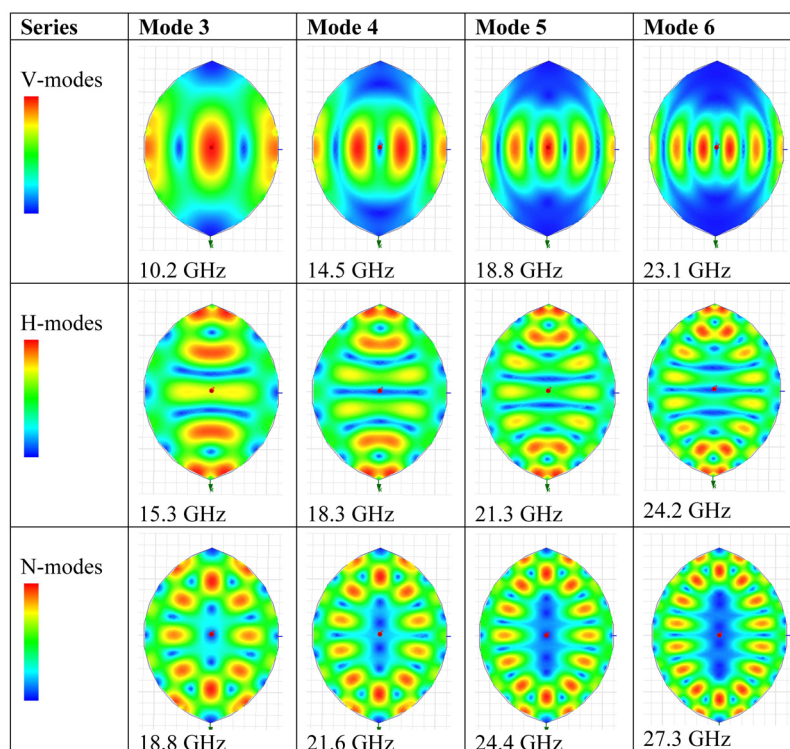


Figure 6: Resonant mode pattern series on model C. Top row shows the electric field strength of the V-mode series. Middle row shows the electric field strength of the H-mode series. Bottom row shows the electric field strength of the N-mode series. Beneath each image the resonant frequency is shown. The bar to the left of each row shows the colour map with red representing highest field strength and blue the lowest.

showed unique pattern modalities, while the three pointed ellipses of model A, B, and C shared similar (but not identical) pattern series (Figure 4). Three of the mode pattern series, referred to here as V-modes ('V' for vertical), H-modes ('H' for horizontal), and N-modes ('N' for node), showed very interesting signatures comparable to real leaf vascular patterns. The progression of these mode pattern series as a function of resonant frequency are shown for model B in Figure 5 and for model C in Figure 6.

The V-mode pattern series was found in all three pointed ellipse models, but not the perfect circle (Figure 4). The V-mode is characterized by equally spaced bands of high electric field strength running parallel to the central longitudinal axis (Figure 5 and 6, top row). As frequency increases, new modes in the V-mode series appear with one additional field maxima (Figure 5 and 6, top row). The V-mode is capable of breaking the symmetry of a homogeneous structure in a manner that is consistent with the vascular patterns observed in monocot leaves of pattern class 1 (Figure 1, top row). A comparison between the 7th V-mode of model B and the leaf of a hosta plant are shown in Figure 7.

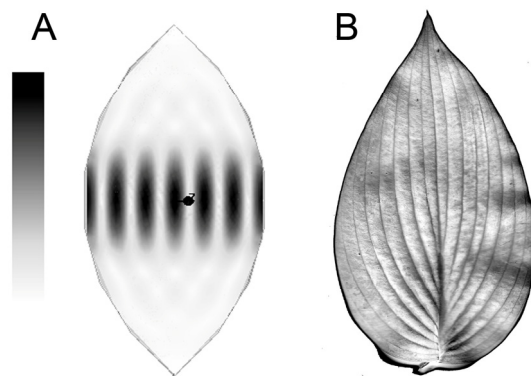


Figure 7: A comparison between the electric field magnitude of the 7th V-mode of model B (40.7 GHz) and the leaf of a pattern series 1 hosta plant (*Hosta capitata*). Scale bar to image left shows electric field strength with black representing high and white low magnitude.

The H-mode pattern series was found in all three pointed ellipse models, but not the perfect circle (Figure 4). The H-mode is characterized by equally spaced bands of high electric field strength running roughly perpendicular to the central longitudinal axis (Figure 5 and 6, middle row and Figure 8). As frequency increases, new modes in the H-mode series appear with one additional field maxima, and at high frequencies field maxima bend into a 'v' shape (Figure 5 and 6, middle row). The H-mode is capable of breaking the symmetry of a homogeneous structure in a manner consistent with the vascular patterns observed in dicot leaves of pattern class 2 (Figure 1, middle row), with an example comparison shown in Figure 8.

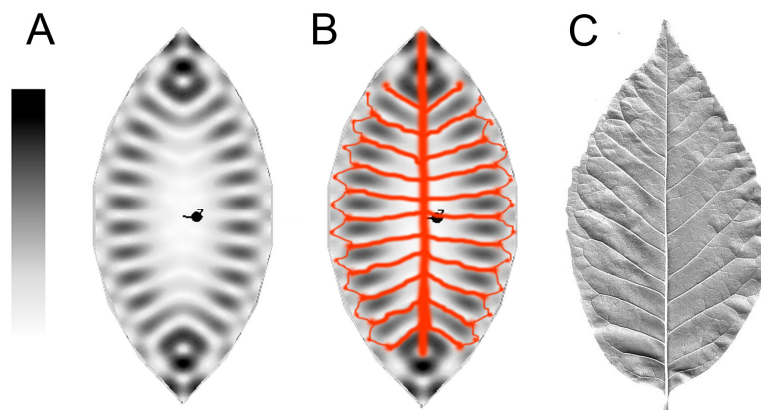


Figure 8: Comparison between the 14th H-mode of model B at 48.4 GHz (panel A), with the vascular structure of a white ash leaf (panel C). The proposed vein development sequence is shown superimposed on the EM mode image in panel B. Scale bar to image left shows electric field strength with black representing high and white low magnitude.

The N-mode pattern series was found in all three pointed ellipse models and in the perfect circle (Figure 4, 5, and 6). The N-mode is characterized by equally spaced nodes of high electric field strength forming around the margin of the structure (Figure 5 and 6, bottom row). As frequency increases, new modes in the N-mode series appear with the addition of two additional field maxima at opposing boundaries (Figure 5 and 6, bottom row). At high frequencies, the H- and N-mode patterns come to appear similar (Figure 6, compare middle and bottom rows). The N-mode is capable of breaking the symmetry of a homogeneous structure in a manner consistent with the vascular patterns observed in dicot leaves of pattern class 2 (Figure 1, middle row). In wider models represented by model C and the perfect circle, the N-mode is capable of selecting multiple axes separated by a fixed angle, which is characteristic of pattern class 3 leaves (Figure 1, bottom row). An example of this capacity is shown in Figure 9, where the 9th N-mode of a circle is shown in comparison to a water lily leaf.

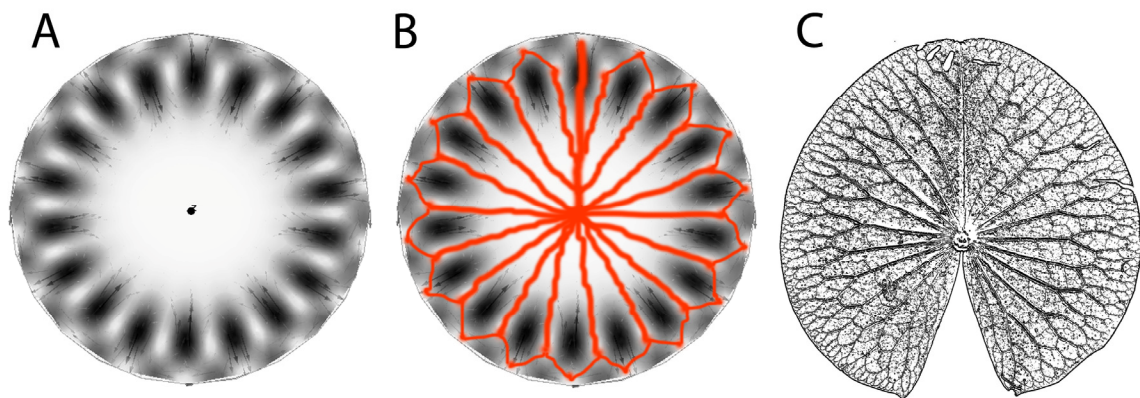


Figure 9: Comparison between the 9th N-mode of a perfect circle (panel A) and the vein structure of water lily leaf (panel C). The proposed vein formation pathway is shown superimposed on the mode image in panel B.

Model A, B, and C all exhibit V-, H-, and N- modes, with only the relative prevalence of particular modes being higher in some models and not others. As a function of frequency, model C showed a higher incidence of V-modes, while models A and B showed higher incidence of H- and N- modes (Figure 4 and Figure 10).

The H- and N- modes appear to influence leaf vascular patterning in a consistent, predictable manner (Figure 11). I hypothesize that the vascular network results from two physical processes. It is hypothesized that first, an EM resonant mode is created which breaks the symmetry of the developing primordium, likely by creating regions of high auxin concentration in relation to electric field strength. Secondly, PIN1 controlled auxin flow from this initial auxin distribution established by the EM resonant mode ultimately leads to differentiation of cells towards vascular tissue. Notably, a central midvein-like feature is not present in any of the resonant mode pattern series shown in Figures 5 and 6. Thus, it is also hypothesized that the midvein of pattern series 2 leaves appears via a mechanism independent of EM-mode formation, perhaps via PIN1-gated auxin flow through the bulk of the leaf and out through the petiole, starting from a homogeneous auxin concentration in the primordium. Comparing plant vascular patterns (Figure 1) and EM resonant modes of the H- and N- series (Figure 5 and 6) implies that secondary veins form in relation to areas of lowest or highest EM field strength. Here it is assumed that veins form in areas of lowest EM field strength. Auxin maxima may form at electric field minima (Figure 11 B). Note that the electric field minima appear in two sets, with fine minima appearing nearest to the boundary and coarse minima (longitudinal bands in H-modes and spots in N-modes) appearing closer to the central region (Figure 11 A and B). It appears as though

secondary veins form along the coarse minima, while the positioning of the fine minima influence the location of secondary vein bifurcation points and can thereby account for a connected network in the leaf margin (Figure 11 C). Examples of this hypothesized vein creation mechanism in relation to EM modes and real leaves are shown in Figure 8 and 9.

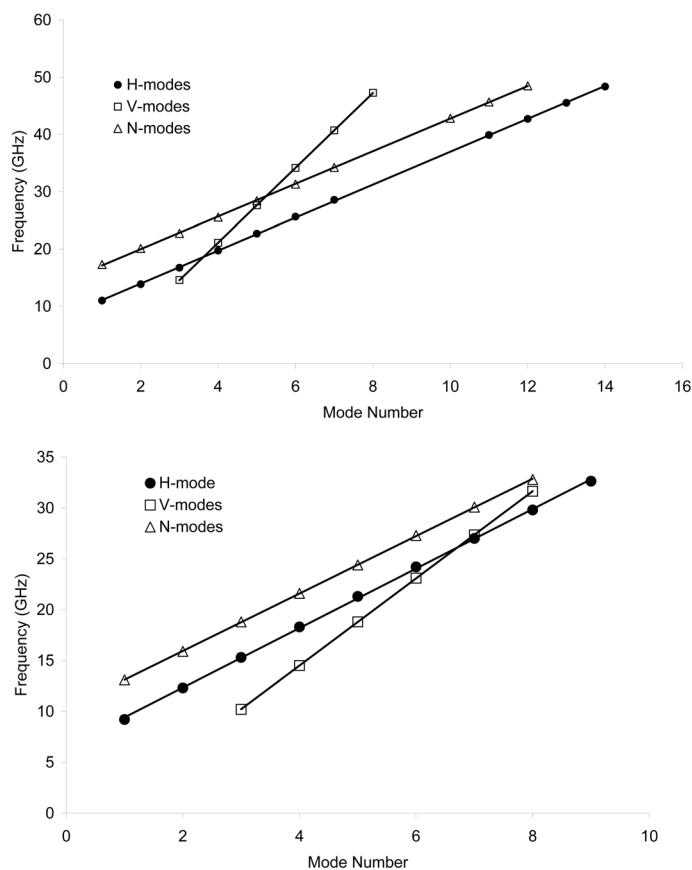


Figure 10: Frequency dependence of V-mode, H-mode, and N-mode pattern series forming on model B (top image) and model C (bottom image). In the wider model C, V-modes are more common at lower frequencies than they are in thinner models B and A. This is indicated by the V-node frequency dependence having a smaller slope in model C than model B.

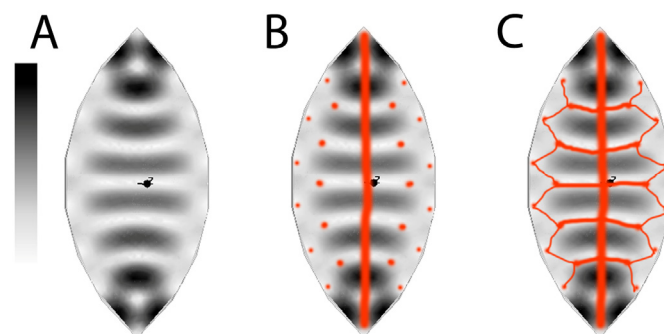


Figure 11: Mechanism of action proposed for H- and N- modes in leaf vascular development. The electric field magnitude of the 6th H-mode of model B is shown in panel A, with field maxima shown in black and minima in white. Panel B shows the primary midvein forming via an alternative mechanism. Auxin maxima are proposed to form in regions of lowest electric field strength (panel B). Connecting regions of high auxin level via a hypothesized auxin canalization mechanism leads to a characteristic leaf vascular pattern (panel C).

Support for this hypothesized relationship between H- and N- modes and leaf vascular network formation exists in the branching characteristics of real leaves (Figure 12). Here the 'margin' is defined in leaves as the distance between the first branch point of a secondary vein and the leaf boundary, and in EM H- and N- modes as the distance between the edge of a course node and the model boundary. Lower frequency H- and N- nodes have a progressively smaller margin size as mode frequency increases and course and fine nodes are pushed towards the outer boundary (compare Figure 12 A-B and E-F, also see Figure 13). This characteristic of H- and N- modes as a function of frequency is consistent with the general behavior of pattern class 2 leaves. As the number of veins (corresponding to mode nodes) gets larger, the margin size tends to decrease dramatically (compare Figure 12 C-D and G-H; also see Figure 13).

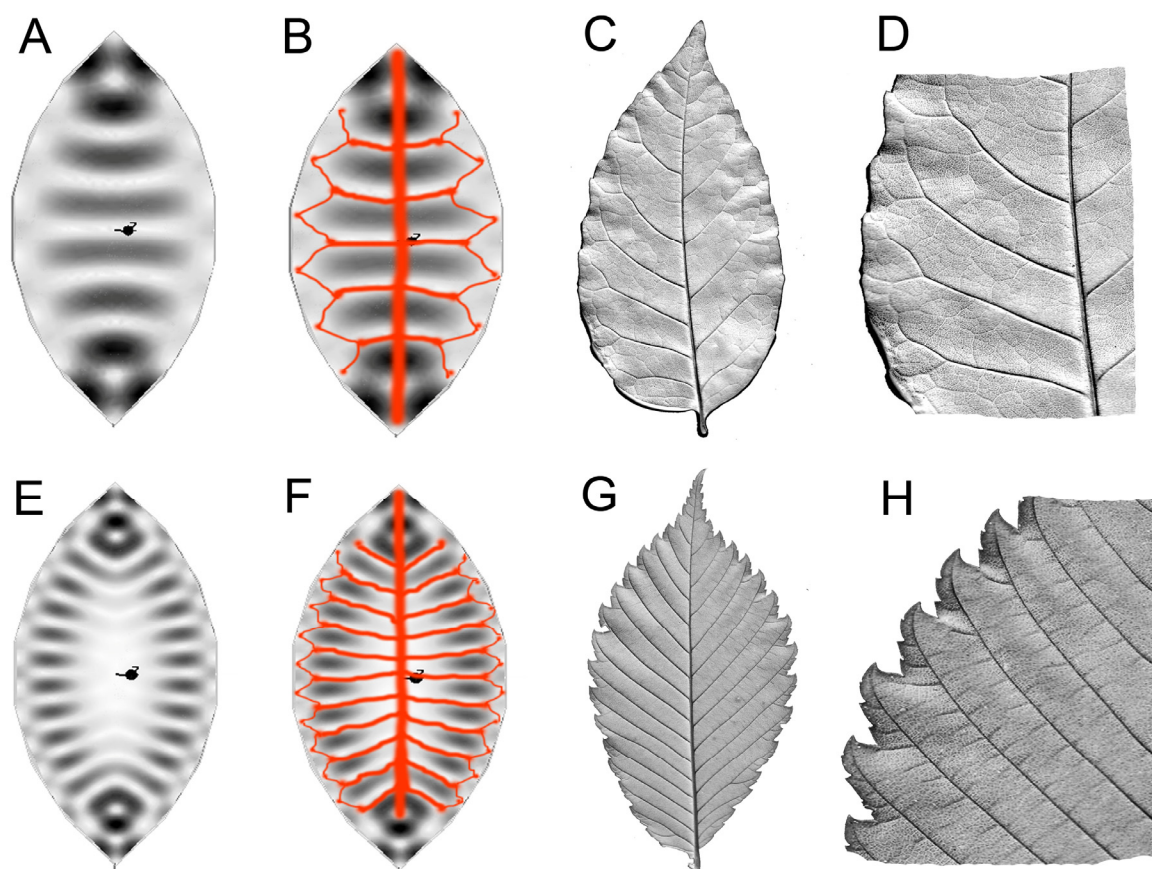


Figure 12: Margin effects in low-frequency (panel A-D) and high frequency (panels E-H) modes and corresponding leaf patterns. Panel A shows the 6th resonant H-mode on model B, while panel B shows the proposed vein creation resulting in large forks due to the positioning of coarse and fine edge nodes. This parallels the margin pattern of an 8 secondary-vein leaf (red ash) shown in panel C with a close up of margin structure in panel D. In contrast, a higher frequency 14th resonant H-mode on model B, with proposed vein creation resulting in smaller forks closer to the boundary due to the positioning of coarse and fine edge nodes (panel F), parallels the 16 secondary-vein leaf (American beech, panel G) and its margin structure (panel H).

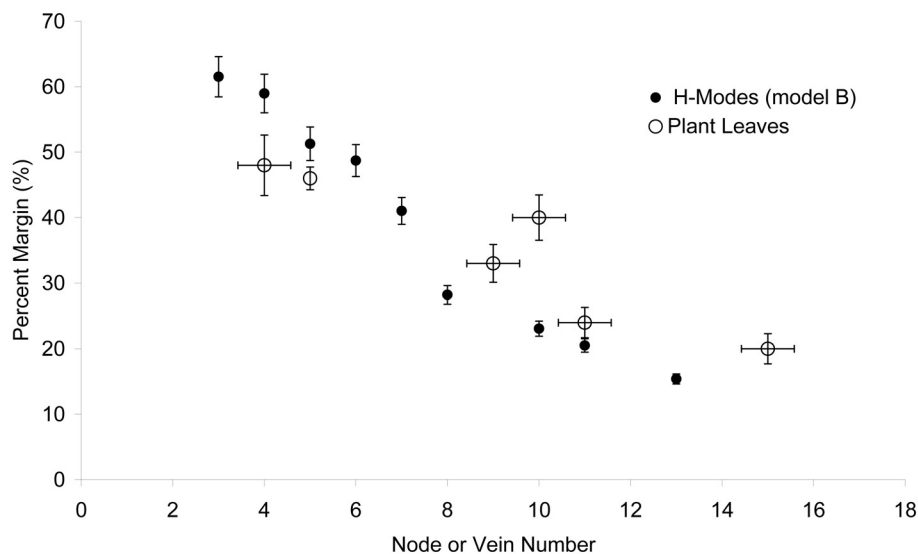


Figure 13: The margin of H-modes decreases with increasing frequency (node number) in a manner paralleling the general behaviour observed in real leaves. The margin is defined as the distance between the boundary and the first bifurcation point of a secondary vein in leaves, or the distance between the boundary and the edge of a course node in resonant H-modes. The percent margin is defined as the percentage distance of the margin distance in relation to the half width of the leaf/mode at its widest point.

4. Discussion

Resonant EM modes forming in a developing biological organ may account for key symmetry breaking events in morphogenesis. Here a FEA model of a rough leaf-primordium-like structure generated three EM resonant mode pattern motifs (the V-, H-, and N- mode series) capable of accounting for basic structural features found in a variety of monocot and dicot leaves. The V- node, consisting of alternating high and low electric field strength bands running parallel to the longitudinal axis of the model, would be capable of symmetry breaking in monocot structures of pattern class 1 leaves. The H- and N- nodes, which appeared similar at higher frequencies, had electric field patterns making them capable of symmetry-breaking in dicot structures of pattern class 2 and 3.

A new hypothesis was also put forth connecting the concept of EM resonant mode activity with more conventional understanding of leaf vascular formation. Here it is proposed that leaf patterns are the consequence of: (i) an the initial symmetry breaking of a homogeneous collective by the electric field of a resonant EM mode, which may influence the initial auxin distribution in the leaf by causing it to form or segregate only in low/high electric field regions, and (ii) the formation of auxin flow paths from this initial auxin distribution via a PIN1 regulated auxin-canalization type mechanism leading to dedicated auxin flow channels that ultimately differentiate into vascular tissue.

Notably, the resonant modes generated on model structures and determined using FEA do not account for all main characteristics of a leaf's vascular pattern. The primary mid-vein of pattern class 2 leaves is not evident in any of the mode series shown in this report. Also, while many dicot leaves have secondary veins with a significant and systematic curvature (Figure 1 and 2 show examples), there is nothing in the horizontal banding patterns of H-modes or the positioning of field nodes/maxima in N-modes, which provides any sign of the curvilinear profile of secondary veins in leaves.

There are numerous deficiencies in the current FEA models which may contribute to inaccuracies such as an inability to account for curvilinear vein profiles. A leaf primordium typically forms as a tissue sheet folded and curved about the meristem into a highly 3-dimensional structure. Also, leaves and leaf primordia are typically more of a teardrop shape with a wider base and pointed tip and are not symmetrical about the horizontal axis like the pointed ellipses modeled here. Therefore, more realistic and complex geometries may need to be modeled to generate resonant modes of greater accuracy and capacity to account for real vein characteristics. In addition, the FEA model considers the leaf tissue to be a homogeneous material, when in fact biological materials at the microscopic scale consist of a variety of parts such as lipid membranes, bound water, and proteins – all of which have significantly different electrical and physical properties. Finally, the FEA model represents a classical solution to Maxwell's equations while the underlying phenomenon of biological coherence rests on a quantum field theory platform. Using a classical model may not account for all features exhibited by the real system, in the same way that modeling a superconductor as an ideal conductor or a superfluid as a zero-viscosity liquid does not yield a complete description of the material and its exhibited phenomena.

5. Conclusions

In conclusion, a finite element analysis model provides electromagnetic mode solutions with standing electric fields sharing key geometric signatures with leaf vascular patterns. The formation of a resonant electromagnetic mode within a developing tissue/organ is therefore capable of explaining how a developing biological system can begin as a homogeneous cell collective and consistently break symmetries in precise ways with global features interrelated in systematic ways. On account of these similarities between this basic model and real leaf patterns, further theoretical and experimental investigations are warranted.

References

1. Pietak, A., *Describing long-range patterns in leaf vasculature with metaphoric fields*. J Theoretical Biology, 2009. **261**: p. 279-289.
2. Jean, R., *Phyllotaxis: The status of the field*. Mathematical biosciences, 1996. **127**: p. 181-206.
3. Koch, A. and H. Meinhardt, *Biological pattern formation: from basic mechanisms to complex structures*. Reviews Mod Phys, 1994. **66**: p. 1481-1494.
4. Meinhardt, H., *Models of biological pattern formation: common mechanisms in plant and animal development*. Int J Dev Biol, 1996. **40**: p. 123-134.
5. Scarpella, E., et al., *Control of leaf vascular patterning by polar auxin transport*. Genes and Development, 2006. **20**: p. 1015-1027.
6. Rolland-Lagan, A. and P. Prusinkiewicz, *Reviewing models of auxin canalization in the context of leaf vein pattern formation in Arabidopsis*. The Plant J, 2005. **44**: p. 854-865.
7. Uggla, C., et al., *Auxin as a positional signal in pattern formation in plants*. PNAS, 1996. **93**: p. 9282-9286.
8. Mitchison, T., *A model for vein formation in higher plants*. Proc Royal Soc London B - Bio Sci, 1980. **207**: p. 79-109.
9. Feugier, F., A. Mochizuki, and Y. Iwasa, *Self-organization of the vascular system in plant leaves: Inter-dependent dynamics of auxin flux and carrier proteins*. J Theor Bio, 2005. **236**: p. 366-375.
10. Rolland-Lagan, A., *Vein patterning in growing leaves: axes and polarities*. Curr Opin Gen Dev, 2008. **18**(4): p. 348-353.
11. Aloni, R., et al., *Gradual shifts in sites of free-auxin production during leaf-primordium development and their role in vascular differentiation and leaf morphogenesis in Arabidopsis*. Planta, 2003. **216**: p. 841-853.
12. Runions, A., et al., *Modeling and visualization of leaf veinination patterns*. ACM Trans Graphics, 2005. **24**: p. 702-711.
13. Staelin, D., A. Morgenthaler, and J. Kong, *Resonators*, in *Electromagnetic Waves*. 1994, Prentice Hall: New Jersey. p. 336-401.
14. Pethig, R. and D. Kell, *The passive electrical properties of biological systems: their significance in physiology, biophysics and biotechnology*. Phys Med Biol, 1987. **32**: p. 933-970.
15. El-Rayes, M. and F. Ulaby, *Microwave dielectric spectrum of vegetation - part I: experimental observations*. IEEE Trans Geosci Remote Sens, 1987. **GE-25**(5): p. 541-549.
16. Gabriel, S. and R. Lau, *The dielectric properties of biological tissue III: Parametric models for the dielectric spectrum of tissues*. Phys Med Biol, 1996. **41**: p. 2271-2293.
17. Frohlich, H., *Long-range coherence and energy storage in biological systems*. International J of Quantum Chemistry, 1968. **2**: p. 641-649.
18. Frohlich, H., *Bose condensation of strongly excited longitudinal electric modes*. Physics Letters A, 1968. **26A**: p. 402-403.
19. Frohlich, H., *Evidence for bose condensation-like excitation of coherent modes in biological systems*. Physics Letters A, 1975. **51A**: p. 21-22.
20. Del Giudice, E., S. Doglia, and M. Milani, *Quantum field theoretical approach to the collective behaviour of biological systems*. Nuclear Physics B, 1985. **B251**: p. 375-400.
21. Del Giudice, E., P. Spinetti, and A. Tedeschi, *Water dynamics at the root of metamorphosis in living organisms*. Water, 2010. **2**: p. 566-586.
22. Preparata, G., *QED Coherence in Matter*. 1995, London: World Scientific. 236
23. Arani, R., et al., *QED coherence and the thermodynamics of water*. Int J of Modern Physics B, 1995. **9**: p. 1813-1841.

24. Cifra, M., et al., *Vibrations of electrically polar structures in biosystems give rise to electromagnetic field: theories and experiments*, in *PIERS Proceedings*. 2009: Moscow, Russia. p. 138-142.
25. Cifra, M., J. Fields, and A. Farhadi, *Electromagnetic cellular interactions*. *Prog Biophys Mol Biol*, 2011. **105**: p. 223-246.
26. Mesquita, M., A. Vasconcellos, and R. Luzzi, *Near dissipationless coherent excitations in biosystems*. *Int J Quant Chem*, 1996. **60**: p. 689-697.
27. Mesquita, M., et al., *Large-scale quantum effects in biological systems*. *Int J Quant Chem*, 2006. **102**: p. 116-1130.
28. Del Giudice, E., S. Doglia, and M. Milani, *Electromagnetic field and spontaneous symmetry breaking in biological matter*. *Nuclear Physics B*, 1986. **B275**: p. 185-199.
29. Smye, S., et al., *The interaction between terahertz radiation and biological tissue*. *Phys Med Biol*, 2001. **46**: p. R101-R112.
30. Brizhik, L., et al., *The role of electromagnetic potentials in the evolutionary dynamics of ecosystems*. *Ecological Modelling*, 2009. **220**: p. 1865-1869.
31. Pietak, A., *Endogenous electromagnetic fields in plant leaves: a new hypothesis for vascular pattern formation*. *Electromag Biol Med*, 2011. **30**(2): p. 93-107.